Journal of Advanced Ceramics
2014, 3(3): 207–214
DOI: 10.1007/s40145-014-0111-3

ISSN 2226-4108
CN 10-1154/TQ

Research Article

Effect of different sol–gel synthesis processes on microstructural and morphological characteristics of hydroxyapatite-bioactive glass composite nanopowders

Mohamadhassan TAHERIAN[a,b,*], Ramin ROJAEE[b,c], Mohammadhossein FATHI[b,c], Morteza TAMIZIFAR[a]

[a]*Department of Materials and Metallurgical Engineering*, *Iran University of Science and Technology* (*IUST*), *Tehran 16866-13114*, *Iran*
[b]*Biomaterials Research Group*, *Department of Materials Engineering*, *Isfahan University of Technology*, *Isfahan 84156-83111*, *Iran*
[c]*Dental Materials Research Center*, *Isfahan University of Medical Sciences*, *Isfahan*, *Iran*

Received: March 15, 2014; Revised: May 31, 2014; Accepted: June 06, 2014

Abstract: The aim of this work was to study the influence of the different synthesis processes on microstructural and morphological characteristics and distribution of hydroxyapatite-bioactive glass (HAp-BG) composite nanopowders obtained by sol–gel method. HAp-BG composite nanopowders with 20 wt% bioactive glass were prepared using a sol–gel method via four routes: (I) mixing the prepared HAp solution with BG solution before aging time; (II) mixing the prepared BG solution with the prepared HAp gel after gelation; (III) mixing the calcined BG nanopowders with the prepared HAp solution; and (IV) mixing the two prepared calcined nanopowders by mechanochemical activation. The prepared nanopowders were evaluated and studied by X-ray diffraction (XRD), scanning electron microscopy (SEM), energy dispersive X-ray spectrometer (EDS), Fourier transform infrared (FTIR), transmission electron diffraction (TEM) and Brunauer–Emmet–Teller (BET) method to investigate the phase structure, microstructure and morphology, functional groups, and the size and distribution of nanopowders. Results indicated that morphology, crystallinity, crystallite size and specific surface area (SSA) of the powders are highly correspondent to the process and type of synthesis method. These findings suggest that the modified sol–gel derived HAp-BG composite nanopowders are expected to efficiently provide a possibility to produce a good candidate to use for fabrication of a bulk nanostructured HAp-BG composite for bone tissue engineering.

Keywords: hydroxyapatite (HAp); bioactive glass (BG); composite; nanopowders; sol–gel

1 Introduction

The hard tissues of bones are composed of calcium phosphate minerals which play vital roles during bone metabolism. These inorganic minerals mechanically support the body and provide the essential ions into the body fluids to maintain homeostasis [1]. A great deal of research has shown that calcium phosphates and their derivatives (such as hydroxyapatite) can provide a desirable environment for bone tissue regeneration due

* Corresponding author.
E-mail: mht.taherian@hotmail.com

to their similarity in chemistry to natural bone, enamel and dentine [2]. Due to the large surface area to volume ratio of nanometer-sized particles, it has been found that nanostructured biomaterials increase mechanical reliability, osteoblast cell adhesion, proliferation and mineralization compared with their conventional micron-scale counterparts [3,4].

A major component of the inorganic part of natural bone is composed of nanostructured hydroxyapatite (HAp, $Ca_{10}(PO_4)_6(OH)_2$) crystals of approximately 50 nm in length and 5 nm in diameter [2]. A successful bone regeneration of the applied biomaterials depends on the cell proliferation, differentiation and mineralization of the extracellular matrix [5]. Nanostructured HAp interacts with osteoblast cells and mimics the structure of the natural extracellular matrix. Moreover, research has shown that the nanocrystalline HAp enhances osteoblast adhesion and proliferation compared to conventional micron-sized HAp [6]. However, medical applications of HAp have been limited because of its low mechanical properties and slow rate of osseointegration [7]. Ideal orthopedic biomaterials should improve the mechanical properties and bioactivity during implantation. Currently, bioactive glass and hydroxyapatite are two main bioactive materials for bone regeneration therapies [8].

Incorporation of bioactive glass (BG) particles endows particular properties to HAp, such as improving bioactivity and mechanical properties [9]. The certain composition of bioactive glasses containing SiO_2–CaO–P_2O_5 has found wide applications as bone implants [10]. Results of *in vivo* implantation show that these compositions bond to tissues without an intervening fibrous layer and produce no local or systemic toxicity [11]. Introduction of silicate ions into the HAp structure improves *in vivo* bioactivity and induces both osteogenesis and angiogenesis during bone regeneration [7,12].

Recently, sol–gel technique as a wet chemical method has been widely applied for synthesis of bioceramic nanopowders. The crystalline degree and morphology of the sol–gel derived nanopowders can be controlled by a number of parameters including the intrinsic properties of the solution (e.g., the type of bioceramics, the conformation of bioceramic concentration) and the operational conditions (e.g., the hydrolysis time, the sequence of reactions) [13,14].

The aim of present research was to evaluate and compare the effect of different synthesis processes on microstructural and morphological characteristics and distribution of hydroxyapatite-bioactive glass (HAp-BG) composite nanopowders obtained by sol–gel method. Based on the obtained results, the optimum process of the preparation could be introduced.

2 Materials and methods

2.1 Powder preparation

The preparation of the sol–gel derived HAp and bioactive glass powders was slightly modified from our previous works and published reports [15–17]. In brief, as sol–gel precursors for HAp, calcium nitrate tetrahydrate ($Ca(NO_3)_2{\cdot}4H_2O$, Merck) and phosphoric pentoxide (P_2O_5, Merck) were used. Both were hydrolyzed separately in ethanol (Et(OH), Merck), and then mixed at a Ca/P ratio of 1.67, and stirred for 2 h. The mixture was continuously stirred for 24 h at ambient temperature. This process was called aging. The gel was dried at 80 ℃ for 24 h.

The bioactive glass was prepared with the nominal composition (in mol%) of 46.1%SiO_2–51.3%CaO–2.6%P_2O_5 by hydrolysis and polycondensation reactions of chemicals using reagent-grade tetraethyl orthosilicate (TEOS, $Si(OC_2H_5)_4$, Merck), triethyl phosphate (TEP, $OP(OC_2H_5)_3$, Merck), calcium nitrate tetrahydrate ($Ca(NO_3)_2{\cdot}4H_2O$, Merck), ethanol (Et(OH), Merck), hydrochloric acid (HCl, Merck) and deionized distilled water. The molar ratio of each compound was adjusted according to the molar ratio of SiO_2, P_2O_5 and CaO within the designed bioactive glass. The precursors were added in sequence and stirred for at least 2 h to prepare a clear solution. The resulting gel was aged at 60 ℃ for 48 h and dried at 120 ℃ for 48 h.

The HAp-BG composite nanopowders were prepared using 20 wt% bioactive glass as reinforcement within the HA matrix by the following different routes:

(I) Mixing HAp solution with BG solution before aging time (HBI);

(II) Mixing BG solution with HAp gel after gelation (HBII);

(III) Mixing calcined BG nanopowders with HAp solution (HBIII);

(IV) Mixing calcined HAp and BG powders by mechanochemical activation (HBIV).

The HBIV sample was produced using a

high-energy planetary ball mill (PM 100, Retsch, Germany) with a zirconia vial and zirconia balls via 2 h mechanochemical activation to produce more homogenous composite nanopowders. Figure 1 outlines the experimental procedure of the present study.

2.2 Powder characterization

Structural changes of the samples (phase composition, crystallinity and crystallite size) were studied by X-ray diffraction analysis (XRD, Philips Xpert, the Netherlands) with Cu Kα radiation ($\lambda = 0.15406$ nm, radiation at 40 kV and 30 mA) over the 2θ range of 20°–70° at a scan rate of 0.02 (°)/s. The obtained experimental patterns were compared to standards compiled by the Joint Committee on Powder Diffraction and Standards (JCDPS), which involved Card No. 9-432 for HAp. The fractions of crystalline phase of HAp in each sample were evaluated using the following equation [18]:

$$X_c = 1 - V_{112/300} / I_{300} \quad (1)$$

where I_{300} is the intensity of the diffraction peak (300) and $V_{112/300}$ is the intensity of the hollow between diffraction peaks (112) and (300) of HAp phase. The size of the HAp crystallites responsible for the Bragg reflection of the (002) and (300) planes was determined using the well-known Scherrer's equation [19]:

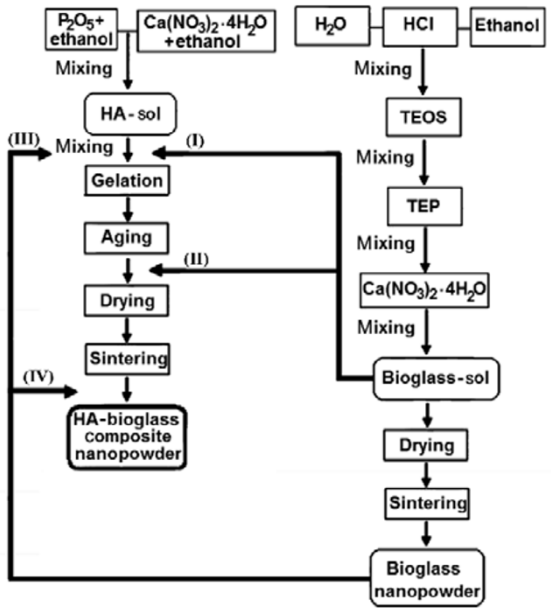

Fig. 1 Schematic illustration of four different preparing routes of composite nanopowders based on sol–gel method.

$$X_s = k\lambda/(B\cos\theta) \quad (2)$$

where X_s is the crystallite diameter (nm); k, λ, B and θ are the shape constant ($k = 0.89$), the wavelength of X-ray beam ($\lambda = 1.5418$ Å for Cu Kα radiation), the full width at half maximum for the diffraction peak (radian), and the diffraction angle (degree), respectively.

The functional groups and chemical structure of the prepared powders were determined by Fourier transform-infrared spectroscopy (FTIR, Jasco-680, Japan). The IR spectra were run on KBr pellets, with a weight ratio of sample to KBr of 1:100. The spectrum was recorded in the range of 4000–400 cm^{-1} with a resolution of 1 cm^{-1}.

The microstructural features and elemental chemical composition of the powders were studied by scanning electron microscopy (SEM, Phillips XL30) attached with an energy dispersive X-ray spectroscopy (EDS, Seron Technology AIS 2300C, Korea) and an image analyzer software (ImageJ, National Institutes of Health, Bethesda, MD, USA).

The morphology and particle size distribution of the powders were carried out by transmission electron microscopy (TEM, LEO 912 AB, Ziess, Germany) in bright field mode, with the accelerating voltage being 120 kV.

The specific surface area (SSA) of the ceramic powders was calculated according to Brunauer–Emmet–Teller (BET) method using Micromeritics Device (Norcross, USA).

The primary particle size (D_{BET}) was estimated by assuming the particles to be spherical [20]:

$$D_{BET} = 6/(\rho S) \quad (3)$$

where ρ is the theoretical density of the sample, and S is the SSA. The ρ value was determined by a precise pycnometeric method according to ASTM D854.

3 Results and discussion

3.1 XRD analyses

Figure 2 shows the XRD patterns of the synthesized composite nanopowders. Since the bioactive glass phase is amorphous, no related peak can be observed in the XRD patterns. Thus the calculated fractions of crystalline phase (X_c) and crystallite size (X_s) of the HAp-BG nanopowders based on the diffraction peaks

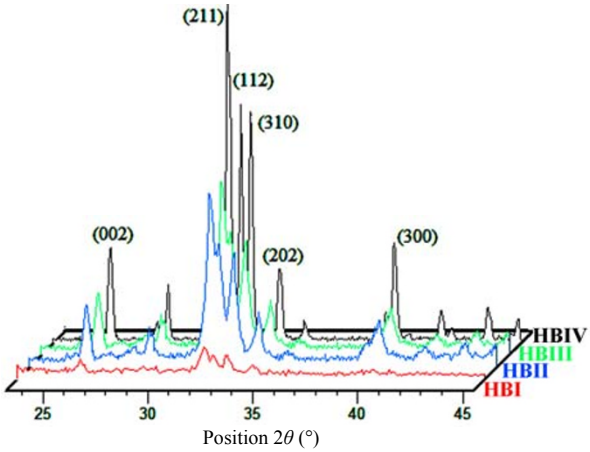

Fig. 2 XRD patterns of HAp-BG composite nanopowders.

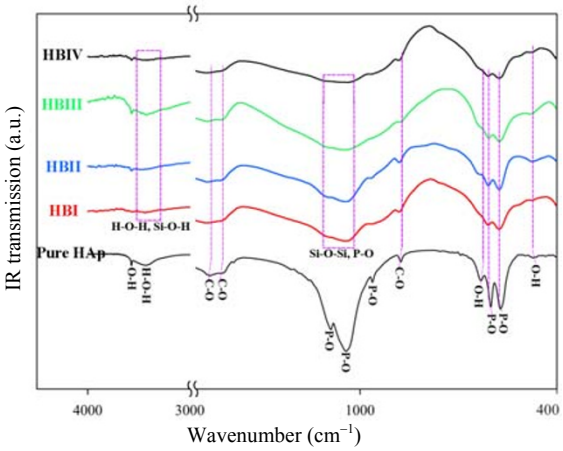

Fig. 3 FTIR spectra of the hydroxyapatite nanopowders and HAp-BG composite nanopowders.

and using Scherrer's formula respectively are listed in Table 1. The XRD investigation reveals that the fraction of crystalline phase of the final composite nanopowders is affected by the sequence of adding precursors. The crystallinity of the composite decreases in the presence of bioactive glass as the sintering temperature was set at 600 ℃ for all the samples. Silicon-containing ionic products of the bioactive glass can easily be released in the HAp sols. Andersson *et al*. [21] reported that the presence of silica in the solution slows down the HAp crystallite growth. Compared to the pure HAp and HAp-BG nanopowders, the composite nanopowders would be restricted in the crystallization owing to silica which acts as a barrier to crystallization against another phase by limiting atomic arrangement [22]. It is worth noting that the difference in crystallinity between HBIV sample and the pure HAp reported by Latifi *et al*. [23], is not distinct. Moreover, *in situ* synthesis (the HAp solutions including BG, i.e., HBI, HBII and HBIII samples) leads to decrease in the crystallite size of HAp-BG nanopowders.

3.2 FTIR spectroscopy

FTIR spectra of the prepared composite nanopowders are presented in Fig. 3. The data obtained for bare pure HAp is also inserted in Fig. 3 for comparison. In general, the spectra do not show significant differences on absorption bands among the composite producing procedures. For all the specimens, the characteristic vibration bands of PO_4^{3-} are observed at around 560–570 cm^{-1}, 600–610 cm^{-1}, 960–970 cm^{-1} and 1000–1100 cm^{-1}, and OH^- bands at around 460–480 cm^{-1}, 620–640 cm^{-1} and 3520–3530 cm^{-1}, showing typical HAp characteristics [16,24,25]. The bands at 3300–3400 cm^{-1} correspond to H–O–H from water absorption of synthesis process [26]. A comparison between pure HAp and HAp-BG composite IR spectra shows that the intensity of characteristic bands decreases in composite nanopowders, which could be attributed to the presence of SiO_2. In the composite nanopowders, the absorption bands around 1000–1100 cm^{-1} correspond to both P–O and Si–O–Si groups. Furthermore, the absorption bands in the range of 3200–3400 cm^{-1} indicating that the Si–OH groups are present in the composite nanopowder lattice structure [17,23]. It should be pointed out that HAp and silica share a number of superimposed vibrational bands, due to similarities of SiO_4^{4-} and PO_4^{3-} tetrahedral molecular units [23,27]. Thus, it would be difficult to distinguish SiO_2 absorption bands because of stronger overlapping absorption bands of HAp.

The characteristic bands of C–O group occur at 860–880 cm^{-1} and 1400–1450 cm^{-1}. A band at about 875 cm^{-1} could be either CO_3^{2-} or HPO_4^{2-} groups. It suggests that CO_3^{2-} ions are partly substituted with PO_4^{3-} in the apatite structure and the amorphous complex [23]. The CO_3^{2-} ions may be resulted from the incomplete pyrolysis of organic compounds or as a common contaminant from the atmosphere. They

Table 1 Crystallinity and crystallite size of hydroxyapatite with 20 wt% bioglass nanopowders

Sample	Crystallite size (nm)	Crystallinity (%)
HBI	28	65
HBII	55	66
HBIII	54	66
HBIV	58	70

possibly penetrate within the composite structure during synthesis process [28,29]. The dissolution of CO_2 from the atmosphere occurs by the following reaction:

$$CO_2(g) + 2OH^-(aq) \rightarrow CO_3^{2-}(aq) + H_2O(l) \quad (4)$$

Since carbonated apatite is more similar to the bone structure, the presence of CO_3^{2-} may improve the bioactivity of the composition [30,31].

3.3 SEM and EDS evaluation

Figure 4 shows the morphological characteristics and elemental analyses of the prepared composite nanopowders. Large platelet or flake shape agglomerates are formed in the HBI sample due to the influence of short-range van der Waals forces during aging [20,32]. The size distribution range of HBI sample particles is approximately 10–300 nm. By changing the synthesis process of composite nanopowders, the plate like aggregates are converted into more uniform distribution of particles, especially for HBII and HBIII samples. The particle size distributions of the HBII, HBIII and HBIV samples are approximately achieved in the range of 15–130 nm, 10–150 nm and 20–350 nm, respectively. Thus, HBIV sample has greater size of agglomerates. This observation could be explained by milling process. During the initial stage of milling, the rate of agglomeration is higher than that of fragmentation of fine particles due to higher rate of cold welding [33]. Generally speaking, the SEM micrographs of all the samples show that plenty of significantly fine particles are interconnected and form irregular agglomerated clusters.

It should be noted that the fine and homogeneous microstructure is the initial important factor for improvement in mechanical properties and biomedical performance of bulk ceramics [34,35].

It has been demonstrated that the morphology and the degree of aggregation are attributed to the concentration and the rate of mixing applied to the solutions. From the view of the mentioned observation, it is expected that since the concentration of primary solutions and the mixing speed of the precursors are low, the final powders are toward the formation of non-agglomerated particles [28], while our observation reveals that the overall mixing procedure is another important factor which determines the morphological characteristics.

Since the bioglass nanopowders are added within the hydroxyapatite solution (HBII and HBIII samples), the HAp nanoparticles start to deposit on the surface of the heterogeneous nucleation sites [36]. It is confirmed that SiO_2 in the bioglass structure can inhibit the HAp particle growth [21,28]. Thus, fine and well distributed spherical shape is produced in the HBII and HBIII samples.

As shown in Fig. 4, the existence of Ca, P, O and Si in the EDS analysis is related to hydroxyapatite and bioactive glass. The EDS result confirms that a homogeneous distribution of components is formed during synthesis. As expected, the elemental components of all the samples are almost the same. EDS analysis also gives the insight into the variations in the composition of Ca/P ratios of the prepared composite nanopowders. Because of the presence of

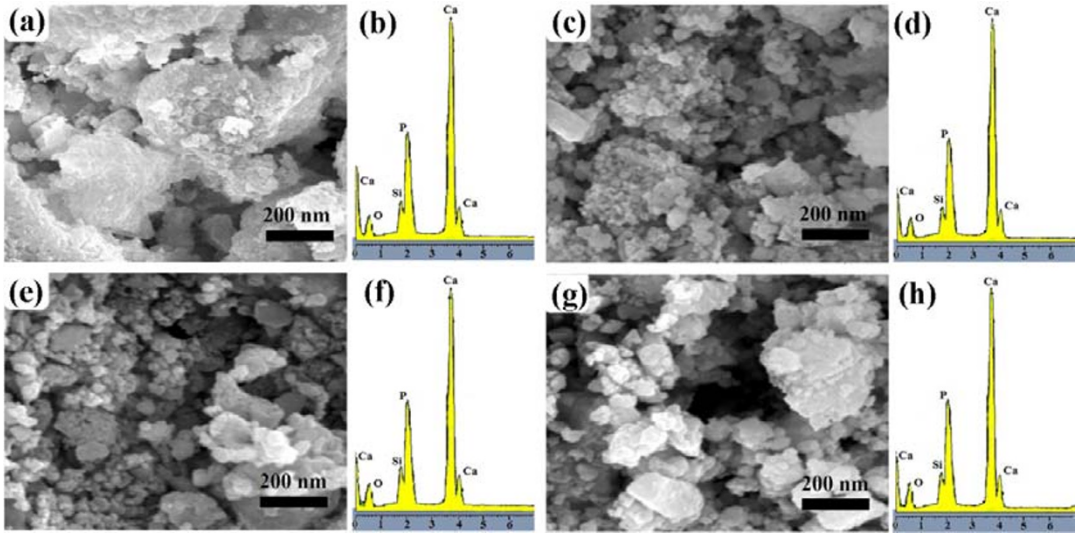

Fig. 4 SEM micrographs and EDS analyses of the ((a) and (b)) HBI, ((c) and (d)) HBII, ((e) and (f)) HBIII, and ((g) and (h)) HBIV samples.

Ca and P in bioactive glass precursors, the ratio of Ca/P is higher than that in pure HAp (> 1.67). Moreover, the Ca/P contents vary in each sample suggesting that the synthesis process modifies the Ca/P ratio.

3.4 TEM analysis

To get a clear insight into the nanostructure nature of the produced composites and also to investigate the particle morphologies, TEM micrographs are provided as shown in Fig. 5. All the samples show nano-sized spheroidal morphology. The powders show a cluster-like structure which is composed of several small particles in the range of 20–60 nm. The agglomerate particles are hard to break down even with long time ultrasonication, especially for HBI and HBII particles. The formation of agglomerated particles can be explained by different possible reaction mechanisms in various synthesis scripts [31]. This confirms the changes in the morphology of the composite nanopowders.

3.5 BET and average grain size

The specific surface area (SSA) values of the composite nanopowders are presented in Table 2. The results of the average particle size (D_{BET}) measurements on these samples are also given. It should be noted that the aggregation of the powders decreases the specific surface area [37]. The calculated D_{BET} ranges between 30 nm and 70 nm. The results are in good agreement with TEM observations and the mean crystallite size determined by XRD. A slight difference between these results is due to assumption of powders to be spherical in BET method. According to the previous investigations, decreasing particle size through increasing the specific surface area would increase the interaction between the material and the physiological solution, and therefore, enhances the kinetics of bioactivity reactions, e.g., osteoblast functions and protein adsorption [38–40].

Table 2 Specific surface area (SSA) and average particle size (D_{BET}) of hydroxyapatite with 20 wt% bioglass nanopowders

Sample	Specific surface area (m^2/g)	Equivalent spherical particle diameter (nm)
HBI	65.49	32.72
HBII	33.56	63.85
HBIII	40.73	52.60
HBIV	32.40	66.12

As a result, we conclude that a reduction of the specific surface area is supported by cluster-like structure formed during powder synthesis methods. Current study has led to the refinement and optimization in the particle size, particle size

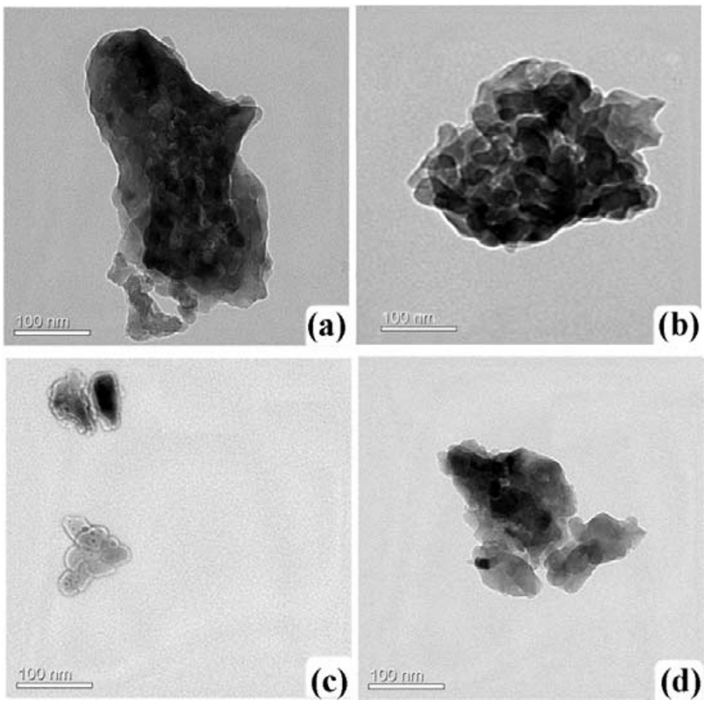

Fig. 5 TEM micrographs of (a) HBI, (b) HBII, (c) HBIII and (d) HBIV samples.

distribution, and degree of particle agglomeration of the HAp-BG composite nanopowders, which are important factors in the selection of the most appropriate biomaterials during tissue interactions. In the next article we will describe our research efforts in two-step sintering process on consolidation of bioactive glass content on sinter-ability, mechanical properties, and bioactivity of hydroxyapatite bulks.

4 Conclusions

In the present study, a comparative study of sol–gel derived hydroxyapatite-bioglass (HAp-BG) composite nanopowders reveals that a number of desirable features in biomaterials can be easily controlled with different processing histories. A uniform microstructure with fine grain size and well distribution is observed for material obtained from route-III processed powders (mixing calcined BG nanopowders with HAp solution), whereas a significant tendency to agglomeration is observed in other powders. The high efficiency of the process opens a way to produce commercial amount of HAp-BG nanopowders. The material can be compacted and transformed in solid HAp-BG ceramic samples which emerge the potential ability to induce bone regeneration when implanted heterotopically. Although further improvements to the HAp-BG composite are necessary, this is a promising first investigation showing its inherent ability to develop in hard tissue applications from the mechanical and biological perspectives.

Acknowledgements

This work was supported by Biomaterials Research Group of Isfahan University of Technology, Iran.

References

[1] Matsunaga K, Murata H, Mizoguchi T, *et al*. Mechanism of incorporation of zinc into hydroxyapatite. *Acta Biomater* 2010, **6**: 2289–2293.

[2] Iskandar ME, Aslani A, Liu H. The effects of nanostructured hydroxyapatite coating on the biodegradation and cytocompatibility of magnesium implants. *J Biomed Mater Res A* 2013 **101A**: 2340–2354.

[3] Webster TJ, Ergun C, Doremus RH, *et al*. Enhanced osteoclast-like cell functions on nanophase ceramics. *Biomaterials* 2001, **22**: 1327–1333.

[4] Catledge SA, Fries MD, Vohra YK, *et al*. Nanostructured ceramics for biomedical implants. *J Nanosci Nanotechno* 2002, **2**: 293–312.

[5] Kharaziha M, Fathi MH, Edris H. Development of novel aligned nanofibrous composite membranes for guided bone regeneration. *J Mech Behav Biomed Mater* 2013, **24**: 9–20.

[6] Hong Z, Mello A, Yoshida T, *et al*. Osteoblast proliferation on hydroxyapatite coated substrates prepared by right angle magnetron sputtering. *J Biomed Mater Res A* 2010, **93**: 878–885.

[7] Xu JL, Khor KA. Chemical analysis of silica doped hydroxyapatite biomaterials consolidated by a spark plasma sintering method. *J Inorg Biochem* 2007, **101**: 187–195.

[8] Xiao XF, Liu RF. Effect of suspension stability on electrophoretic deposition of hydroxyapatite coatings. *Mater Lett* 2006, **60**: 2627–2632.

[9] Sebdani MM, Fathi MH. Preparation and characterization of hydroxyapatite–forsterite–bioactive glass nanocomposite coatings for biomedical applications. *Ceram Int* 2012, **38**: 1325–1330.

[10] Balamurugan A, Balossier G, Michel J, *et al*. Sol gel derived SiO_2–CaO–MgO–P_2O_5 bioglass system—Preparation and *in vitro* characterization. *J Biomed Mater Res B*: *Appl Biomater* 2007, **5**: 546–553.

[11] Sepulveda P, Jones JR, Hench LL. Bioactive sol–gel foams for tissue repair. *J Biomed Mater Res A* 2002, **59**: 340–348.

[12] Zhai W, Lu H, Chen L, *et al*. Silicate bioceramics induce angiogenesis during bone regeneration. *Acta Biomater* 2012, **8**: 341–349.

[13] Wang F, Li M, Lu Y, *et al*. A simple sol–gel technique for preparing hydroxyapatite nanopowders. *Mater Lett* 2005, **59**: 916–919.

[14] Boonstra AH, Bernards TNM. The dependence of the gelation time on the hydrolysis time in a two-step SiO_2 sol–gel process. *J Non-Cryst Solids* 1988, **105**: 207–213.

[15] Rojaee R, Fathi M, Raeissi K. Controlling the degradation rate of AZ91 magnesium alloy via sol–gel derived nanostructured hydroxyapatite coating. *Mat Sci Eng C* 2013, **33**: 3817–3825.

[16] Rojaee R, Fathi M, Raeissi K. Electrophoretic deposition of nanostructured hydroxyapatite coating on AZ91 magnesium alloy implants with different

surface treatments. *Appl Surf Sci* 2013, **285**: 664–673.

[17] Rojaee R, Fathi M, Raeissi K, *et al*. Electrophoretic deposition of bioactive glass nanopowders on magnesium based alloy for biomedical applications. *Ceram Int* 2014, **40**: 7879–7888.

[18] Landi E, Tampieri A, Celotti G, *et al*. Densification behaviour and mechanisms of synthetic hydroxyapatites. *J Eur Ceram Soc* 2000, **20**: 2377–2387.

[19] Fathi MH, Hanifi A, Mortazavi V. Preparation and bioactivity evaluation of bone-like hydroxyapatite nanopowder. *J Mater Process Tech* 2008, **202**: 536–542.

[20] Hidouri M, Bouzouita K, Kooli F, *et al*. Thermal behaviour of magnesium-containing fluorapatite. *Mater Chem Phys* 2003, **80**: 496–505.

[21] Andersson J, Areva S, Spliethoff B, *et al*. Sol–gel synthesis of a multifunctional, hierarchically porous silica/apatite composite. *Biomaterials* 2005, **26**: 6827–6835.

[22] Kim H-W, Kim H-E, Salih V, *et al*. Hydroxyapatite and titania sol–gel composite coatings on titanium for hard tissue implants; Mechanical and *in vitro* biological performance. *J Biomed Mater Res B*: *Appl Biomater* 2005, **72B**: 1–8.

[23] Latifi SM, Fathi MH, Golozar MA. Preparation and characterisation of bioactive hydroxyapatite–silica composite nanopowders via sol–gel method for medical applications. *Adv Appl Ceram* 2011, **110**: 8–14.

[24] Wang J, Chao Y, Wan Q, *et al*. Fluoridated hydroxyapatite coatings on titanium obtained by electrochemical deposition. *Acta Biomater* 2009, **5**: 1798–1807.

[25] Fathi MH, Zahrani ME. Mechanical alloying synthesis and bioactivity evaluation of nanocrystalline fluoridated hydroxyapatite. *J Cryst Growth* 2009, **311**: 1392–1403.

[26] Peon E, Fuentes G, Delgado JA, *et al*. Preparation and characterization of porous blocks of synthetic hydroxyapatite. *Latin Am Appl Res* 2004, **34**: 225–228.

[27] Bianco A, Cacciotti I, Lombardi M. Si-substituted hydroxyapatite nanopowders: Synthesis, thermal stability and sinterability. *Mater Res Bull* 2009, **44**: 345–354.

[28] Moghimian P, Najafi A, Afshar S, *et al*. Effect of low temperature on formation mechanism of calcium phosphate nano powder via precipitation method. *Adv Powder Technol* 2012, **23**: 744–751.

[29] Rojaee R, Fathi MH, Raeissi K. Nanostructured hydroxyapatite coating for biodegradability improvement of magnesium-based alloy implant. In *Advances in Bio-Mechanical Systems and Materials-Advanced Structured Materials*. Ochsner A, Altenbach H, Eds. Springer International Publishing, 2013: 25–40.

[30] Ye H, Liu XY, Hong HP. Cladding of titanium/fluorapatite composites onto Ti6Al4V substrate and the *in vitro* behaviour in the simulated body fluid. *Appl Surf Sci* 2009, **255**: 8126–8134.

[31] Mostafa NY, Hassan HM, Mohamed FH. Sintering behavior and thermal stability of Na^+, SiO_4^{4-} and CO_3^{2-} co-substituted hydroxyapatites. *J Alloys Compd* 2009, **479**: 692–698.

[32] Mayr H, Ordung M, Zieglerc G. EPD of a nanoscale HA powder for biomedical applications. *2nd International Conference on Electrophoretic Deposition*: *Fundamentals and Applications*, 2005.

[33] Fathi MH, Zahrani EM. Fabrication and characterization of fluoridated hydroxyapatite nanopowders via mechanical alloying. *J Alloys Compd* 2009, **475**: 408–414.

[34] Nasiri-Tabrizi B, Fahami A, Ebrahimi-Kahrizsangi R, *et al*. A study on mechanochemical behavior of $CaO–P_2O_5–CaF_2–ZrO_2$ system to produce fluorapatite–zirconia composite nanopowders. *Powder Technol* 2013, **243**: 59–70.

[35] Esnaashary M, Fathi M, Ahmadian M. The effect of the two-step sintering process on consolidation of fluoridated hydroxyapatite and its mechanical properties and bioactivity. *Int J Appl Ceram Tec* 2014, **11**: 47–56.

[36] Nathanael AJ, Lee JH, Mangalaraj D, *et al*. Multifunctional properties of hydroxyapatite/titania bio-nano-composites: Bioactivity and antimicrobial studies. *Powder Technol* 2012, **228**: 410–415.

[37] Zhai W, Lu H, Wu C, *et al*. Stimulatory effects of the ionic products from Ca–Mg–Si bioceramics on both osteogenesis and angiogenesis *in vitro*. *Acta Biomater* 2013, **9**: 8004–8014.

[38] Gupta G, El-Ghannam A, Kirakodu S, *et al*. Enhancement of osteoblast gene expression by mechanically compatible porous Si-rich nanocomposite. *J Biomed Mater Res B*: *Appl Biomater* 2007, **81**: 387–396.

[39] López-Noriega A, Arcos D, Izquierdo-Barba I, *et al*. Ordered mesoporous bioactive glasses for bone tissue regeneration. *Chem Mater* 2006, **18**: 3137–3144.

[40] Ghomi H, Fathi MH, Edris H. Fabrication and characterization of bioactive glass/hydroxyapatite nanocomposite foam by gelcasting method. *Ceram Int* 2011, **37**: 1819–1824.